NASA-CR-194140

FINAL TECHNICAL REPORT

FOR
NCC3 150

ADAPTIVE CONTROL OF INTERFACE BY TEMPERATURE AND INTERFACE PROFILE FEEDBACK IN TRANSPARENT MULTI-ZONE CRYSTAL GROWTH FURNACE

BY

CELAL BATUR
DEPARTMENT OF MECHANICAL ENGINEERING
THE UNIVERSITY OF AKRON
AKRON OHIO 44325-3903

PERIOD 9/25/89 THROUGH 9/24/90
AND
9/1/90 THROUGH 5/31/91

NASA TECHNICAL OFFICER

BRUCE N. ROSENTHAL
PROCESSING SCIENCE AND TECHNOLOGY BRANCH
MAIL STOP 105-1

TOTAL $34,012.00

(NASA-CR-194140) ADAPTIVE CONTROL OF INTERFACE BY TEMPERATURE AND INTERFACE PROFILE FEEDBACK IN TRANSPARENT MULTI-ZONE CRYSTAL GROWTH FURNACE Final Technical Report, 25 Sep. 1989 - 31 May 1991 (Akron Univ.) 32 p

N94-13253

Unclas

G3/63 0182807

PRECEDING PAGE BLANK NOT FILMED

1. OBJECTIVE

The objective of this research is to control the dynamics of multizone programmable crystal growth furnaces. Due to the inevitable heat exchange among different heating zones and the transient nature of the process, the dynamics of multizone furnaces is time varying, distributed and therefore complex in nature.

Electrical power to heating zones and the translational speed of the ampoule are employed as inputs to control the dynamics. Structural properties of the crystal is the ultimate aim of this adaptive control system. These properties can be monitored in different ways. Following an order of complexity, these may include :

a. - on line measurement of the material optical properties such as the refractive index of crystal,

b. - on line X-ray imaging of the interface topology,

c. - on line optical quantification of the interface profile such as the determination of concavity or convexity of the interface shape, and finally,

d.- on line temperature measurement at points closest to the material such as measurements of the ampoule's outside and inside surface temperatures.

The research performed makes use of the temperature and optical measurements, specified in (c) and (d) above as the outputs of furnace dynamics. However, if the instrumentation is available, the proposed control methodology can be extended to the measurements listed in (a) and (b).

2. ACCOMPLISHED RESULTS

Following results are accomplished in this study.

A - Design, construction and validation of a computerized 8 zone heater drive and monitor system. The system has the following technical specifications.

Power drive capacity : 2400 W

Temperature reading resolution : 16 bits for 0 to

1500 C temperature range. This corresponds to 0.02 C

temperature reading resolution.

Heater drive resolution : 16 bits.

Temperature accuracy at the highest setting : 1 C.

Optical resolution of the interface detection : 12 bits

B - Experimental identification of multivariable furnace dynamics.

Pseudo random binary heating power is introduced to the furnace. The multivariable transfer function of the furnace is determined between the input and the resulting zone temperatures.

C - Based on the identified model structure, design and verification of a multivariable controller is accomplished.

3. INTRODUCTION

One common way to grow crystal is to subject the molten material to a temperature gradient. This requires keeping a predetermined axial and radial temperature profile around the material despite the effects of unknown process disturbances. To maintain continuous solidification, either the material or the temperature gradient is moved axially. At any given point, the temperature is a function of axial position h, radial position r, circumferential position c, and the time t. This distributed nature of the temperature can be described by a multivariable function

$$T = T(h,r,c,t)$$

The time dependency of the temperature is due to the following factors:

i- the translational motion of the ampoule with respect to furnace,

ii- the inevitable heat exchange between different heating zones.

The temperature control problem can now be described as follows. Determine the electrical heating power to individual heating zones and the translational motion velocity of the ampoule such that at each point within the ampoule the temperature, $T(h,r,c,t)$, is kept at the desired level, $T_d(h,r,c,t)$,i.e,

$$T(h,r,c,t) = T_d(h,r,c,t)$$

Previous research has shown that the shape of the solid liquid interface is strongly correlated to the imposed temperature gradient and the translational motion velocity of the ampoule. Furthermore, the macroscopic shape of the interface affects the crystalline perfection of the material. It is known that [Chang and Wilcox 1974] minimization of thermal stresses can be achieved by maintaining a planar interface between the solid and the liquid phases of the material. Such planar interface is desirable because crystalline imperfections are also minimized. [Taghavi and Duval 1989] have studied the effects of furnace temperature profile and translational velocity on the interface shape, and they have also considered the inverse problem of the

desired temperature profile that would result in a planar interface. These studies have given insight into the problem of achieving planar interface during crystal growth . Most importantly, the ability to design a furnace where the temperature profile can be tailored during the growth of the crystal is found to be highly desirable for obtaining a planar interface. This has led into the concept of transparent multi-zone Bridgman furnace.

Experimental observations confirm that the same factors affect the shape of interface, namely :

a. the axial temperature profile alongside the ampoule,

b. the radial temperature profile surrounding the interface, and

c. the translational velocity of the ampoule.

[Wang et al 1984] experimented with a single zone vertical Bridgman type furnace using Gallium doped Germanium as the material. They considered the energy flow, the temperature distribution and the translational speed as their main parameters. They verified that the macroscopic growth rate was always transient and the interface remained concave with respect to solid at the translational speed of 4 micro meter/sec. They further concluded that the main parameters effecting the crystal growth process are :

i) the establishment of a well defined and symmetrical temperature profile around the ampoule, and

ii) the provision for the growth interface quantification and control.

The Mellen EDG furnace [Parsey and Thiel 1985] can emulate the heat flow characteristics of the horizontal Bridgman-Stockbarger furnace without requiring the motion of the ampoule. The use of the Mellen furnace in horizontal configuration for a large diameter Gallium Arsenide crystal has been investigated by [Bourret et al 1987]. They have found that the crystalline perfection is improved by increasing the axial temperature gradient over the solid and decreasing the radial temperature gradient over the melt.

Quantification of solid-liquid interface by image processing has been performed by [Batur et al 1990a, 1990b]. This powerful technique can locate the position of interface and determine its concavity or convexity for transparent furnace and materials. This topological information about the interface can serve the following purpose.

- It provides continuous on line information for the position and the shape of the interface. Therefore the effects of different temperature gradients and the translational speeds on the interface can be quantified in real time.

- It can be used as the feedback signal in conjunction with the classical temperature feedback from each zone.

In conclusion, material structural properties, partially observed by the shape of solid-liquid interface, are complex, time dependent phenomena of the temperature profiles and the ampoule's translational velocity. A multivariable experimental furnace model explaining the interactions between different heating zones and the effect of the translational velocity is the first fundamental step to understand the process. The purpose of the proposed investigation is to find this model in real time and based on the model, implement an adaptive multivariable control algorithm for temperatures and interface profile.

4. CRYSTAL GROWTH CONTROL

Control of crystal growth should ideally be based on the desired structural properties of a given material. For example, if the acousto-optical properties of the material are critical then the control law should be designed around these parameters. On line measurement of the solid's refractive index, for example, provides such a feedback signal for the control algorithm. However if the desired structural properties can not be directly measured because of cost or furnace design, then two alternative options exist. If the relation between the desired state and a physically realizable measurement is known then this relation can be used to find the desired measurement. If this relation is unknown, the next best measurement, closest to the desired observation should be provided for the controller.

The shape of the interface is one measurement which is closely related to the structural properties of the material. X-ray imaging of the ampoule, for example, may provide information to determine the solid-liquid interface. The differences in X-ray intensities corresponding to solid and melt can be exploited to determine the topology of the interface. X-ray imaging is an elaborate and equipment intensive process. For transparent furnace and material, if there is significant difference in gray levels or colors between the solid and the melt, optical imaging can also locate the position and the shape of the interface [Batur et al 1990a,1990b].

Perhaps the most practical furnace control methodology is to measure and control the temperatures which define the necessary thermal gradient for the growth of the crystal. Although this control technique is not based on the measurement of the desired structural properties of the material, nevertheless it is preferred for the following reasons.

- As outlined in the introduction, analytical studies have shown that the shape of the interface can be related to the axial and radial temperature distribution surrounding the interface.

- Temperature measurement technology is well established and reliable in comparison with, for example, optical measurements related to the crystal properties.

In the next section we will describe temperature based control methodologies for the crystal growth furnace.

5. CONTROL ALGORITHM

Problem Formulation

The system to be controlled is assumed to have the following model structure

$$A(z^{-1})y(t) = B(z^{-1})u(t) + C(z^{-1})n(t) \quad (1)$$

where

$A(z^{-1}) = I+A_1z^{-1}+A_2z^{-2}+....+A_{na}z^{-na}, \quad A_i \text{ e } \mathbf{R}^{pxp}$

$B(z^{-1}) = B_0z^{-k}+B_1z^{-k-1}+.....+B_{nb}z^{-k-nb}, \quad B_i \text{ e } \mathbf{R}^{pxp}$

$C(z^{-1}) = I+C_1z^{-1}+C_2z^{-2}+.....+C_{nc}z^{-nc}, \quad C_i \text{ e } \mathbf{R}^{pxp}$

where u(t), y(t) and n(t) are p x 1 vectors representing input, output and the disturbance of the system. k is the process dead time. The polynomial $A(z^{-1})$, $B(z^{-1})$, $C(z^{-1})$ may be time varying.

The resulting control law takes the following form.

$$R(z^{-1})u(t) = T(z^{-1})r(t) - S(z^{-1})y(t) \quad (2)$$

where $R(z^{-1})$, $T(z^{-1})$, $S(z^{-1})$ matrix polynomials are designed in such a way to achieve desired characteristics as discussed later and they are assumed to take the following form

$R(z^{-1}) = I+R_1z^{-1}+R_2z^{-2}+....+R_{nr}z^{-nr}, \quad R_i \text{ e } \mathbf{R}^{pxp}$

$T(z^{-1}) = T_0+T_1z^{-1}+T_2z^{-2}+....+T_{nt}z^{-nt}, \quad T_i \text{ e } \mathbf{R}^{pxp}$

$S(z^{-1}) = S_0+S_1z^{-1}+S_2z^{-2}+....+S_{ns}z^{-ns}, \quad S_i \text{ e } \mathbf{R}^{pxp}$

r(t) is the desired reference level of the controller.

Given the system as in (1), it is desired to find a self-tuning control law as in equation (2), so as to make the input sequence u(t) and the tracking error e(t) defined as [r(t) - y(t)] as stable sequences, independent of $C(z^{-1})n(k)$ and r(k). It is also assumed that A, B, C may be slowly time varying.

Controller Design Problem

The closed loop equation is obtained using equation (1) and (2) as

$$Ay = BR^{-1}(Tr - Sy) + Cn$$

$$(A + BR^{-1}S)\, y = BR^{-1}Tr + Cn \tag{3}$$

The dynamics of the closed loop system is dictated by $(A + BR^{-1}S)$ matrix polynomial. This can be made equal to any desired polynomial by suitably choosing R and S. Unfortunately, in trying to obtain R and S using the above method, we end up with a set of non-linear equations and there are no standard techniques to solve this type of equation. Hence, the following transformation is performed

$$R^{-1}S = \tilde{S}\tilde{R}^{-1} \tag{4}$$

[Wolovich 1974] has shown that equation (4) has an unique solution if $\tilde{R}$ and $\tilde{S}$ are given as

$$\tilde{R} = I + \tilde{R}_1 z^{-1} + \ldots + \tilde{R}_{nr} z^{-nr}, \quad \tilde{R}_i \in \mathbf{R}^{pxp}$$

$$\tilde{S} = I + \tilde{S}_1 z^{-1} + \ldots + \tilde{S}_{nr} z^{-nr}, \quad \tilde{S}_i \in \mathbf{R}^{pxp}$$

From equation (4), it follows

$$\frac{adj(R)\, S}{det(R)} = \frac{\tilde{S}\, adj(\tilde{R})}{det(\tilde{R})} \tag{5}$$

Hence

$$det(R) = det(\tilde{R}) \tag{6}$$

because R and $\tilde{R}$ have the identity matrix as its first coefficient. From (4) and (6), it follows

$$det(S) = det(\tilde{S}) \tag{7}$$

Using transformation (4) in (3), we obtain

$$(A + B\tilde{S}\tilde{R}^{-1})y = BR^{-1}Tr + Cn$$

$$(A\tilde{R} + B\tilde{S})\, \tilde{R}^{-1}y = BR^{-1}Tr + Cn \tag{8}$$

In the pole placement procedure, $\tilde{R}$ and $\tilde{R}$ are found to satisfy the following design equations

$$A\tilde{R} + B\tilde{S} = P \tag{9}$$

where P is the desired polynomial matrix. As observed in (8), the dynamics of the closed loop system is also described by $\tilde{R}^{-1}$. In the later section, it is shown that this does not affect the stability of the closed loop system, even though $\tilde{R}$ itself may be unstable.

The main idea behind this algorithm is to solve for $\tilde{R}$ and $\tilde{S}$ matrices in equation (9) and then use these to find R and S using (4). Before getting into details of the solution to equations (4) and (9), let us consider the steady state performance of the

regulator. In order to have no steady state error, R matrix is forced to have an integrator in each loop as given by

$$R(z^{-1}) = (1-z^{-1})R'(z^{-1}) \tag{10}$$

As mentioned before, we have no direct method to select R matrix and its value is determined through $\tilde{R}$. Fortunately equation (6) comes to the rescue, which essentially states that the roots of characteristic equations of R and $\tilde{R}$ matrices are the same. Hence $\tilde{R}$ also has a forced integrator and is given as

$$\tilde{R}(z^{-1}) = (1-z^{-1})\tilde{R}'(z^{-1}) \tag{11}$$

with

$$\tilde{R}' = I+\tilde{R}'_1 z^{-1}+....+\tilde{R}'_{nr-1}z^{-nr-1}, \quad \tilde{R}'_i \text{ e } R^{pxp}$$

Now the steady state conditions for step inputs in r(t) is obtained from equation (8) by considering the limit z -> 1. From equation (11), it follows that $\tilde{R}$ tends to zero when z -> 1. Hence the steady state conditions are given as

$$[A(1)\tilde{R}(1)+B(1)\tilde{S}(1)]\ \tilde{R}^{-1}(1)\bar{y}(t) = B(1)R^{-1}(1)T(1)\bar{r}(t) \tag{12}$$

$$B(1)\tilde{S}(1)\tilde{R}^{-1}(1)\bar{y}(t) = B(1)R^{-1}(1)T(1)\bar{r}(t) \tag{13}$$

Applying transformation in equation (4) to (13), we get

$$B(1)R^{-1}(1)S(1)\bar{y}(t) = B(1)R^{-1}(1)T(1)\bar{r}(t) \tag{14}$$

Hence

$$\bar{y}(t) = S^{-1}(1)T(1)\bar{r}(t) \tag{15}$$

Now the steady state tracking error is given as

$$\bar{e}(t) = \bar{r}(t) - \bar{y}(t) = [I - S^{-1}(1)T(1)]\bar{r}(t) \tag{16}$$

$$\bar{e}(t) = S^{-1}(1)[S(1) - T(1)]\bar{r}(t) \tag{17}$$

Again T matrix is selected such that

$$T(1) = S(1) \tag{18}$$

As a result of the above constraint on T

$$\bar{e}(t) = 0 \tag{19}$$

Instead of just satisfying equation (18), we pick T as

$$T(z^{-1}) = S(z^{-1}) \tag{20}$$

Although this ensures zero steady state error for step inputs, the excess freedom in choosing T matrix is not properly utilized. [Mikles 1990] exploited this to follow ramp and other higher order inputs. At this point, it is just noted that this technique can be modified for higher order reference tracking problems.

Solution to Design Equations

$\tilde{R}$ and $\tilde{S}$ are found by solving (9) with $\tilde{R}$ having the form as in (11). Substituting (11) in (9), we get

$$A\tilde{R}'(1-z^{-1}) + B\tilde{S} = P \tag{21}$$

This can be solved by using Toeplitz form to represent the above relation. Introducing

$$A_v = \begin{Bmatrix} 0_1 \\ \cdots \\ 0_v \\ I \\ A_1\text{-}I \\ A_2\text{-}A_1 \\ \cdots \\ A_{na}\text{-}A_{na-1} \\ -A_{na} \\ 0_{na+v+2} \\ \cdots \\ 0_{np} \end{Bmatrix} \quad B_v = \begin{Bmatrix} 0_1 \\ \cdots \\ 0_k \\ B_0 \\ B_1 \\ B_2 \\ \cdots \\ B_{nb-1} \\ B_{nb} \\ 0_{nb+k+v} \\ \cdots \\ 0_{np} \end{Bmatrix} \tag{22}$$

where np is the order of P matrix and each 0_i is a pxp null matrix. Then the system denoted in (21) is given by

$$[A_0 \ldots A_{nr-1} B_0 \ldots B_{ns}] \begin{pmatrix} \tilde{R}_1' \\ \tilde{R}_2' \\ \ldots \\ \tilde{R}_{nr}' \\ \tilde{S}_0 \\ \tilde{S}_1 \\ \cdots \\ \tilde{S}_{ns} \end{pmatrix} = \begin{pmatrix} P_1 \\ P_2 \\ .. \\ .. \\ .. \\ .. \\ P_{np-1} \\ P_{np} \end{pmatrix} \begin{pmatrix} A_1\text{-}I \\ A_2\text{-}A_1 \\ \cdots \\ A_{na}\text{-}A_{na-1} \\ -A_{na} \\ 0_{na+2} \\ \cdots \\ 0_{np} \end{pmatrix} \tag{23}$$

This is a linear system of equation and solutions to such equations are well known. In particular, LU decomposition is used to solve for the unknown matrices.

In a similar fashion equation (4) is solved with R having a form as (10) and $\tilde{R}$ satisfying (11). Substituting relations (10) and (11) in (4), the following result is obtained.

$$(1-z^{-1})^{-1}R'^{-1}S = \tilde{S}\tilde{R}'^{-1}(1-z^{-1})^{-1} \tag{24}$$

Cancelling the common terms in (24), we obtain

$$R'^{-1}S = \tilde{S}\tilde{R}'^{-1} \tag{25}$$

It can be seen that (25) is similar to (4). Rearranging and then taking transpose, equation (25) takes the following form

$$\tilde{R}'^{T}S^{T} - \tilde{S}^{T}R'^{T} = 0 \tag{26}$$

Here $\tilde{R}'$, $\tilde{S}$ are known quantities and R', S are the unknown quantities for which the equation has to be solved. This equation is similar to (21) and hence adapting a similar procedure, we define the following matrices,

$$R_v^T = \begin{Bmatrix} 0_1 \\ \cdots \\ 0_v \\ I \\ \tilde{R}_1'^T \\ \cdots \\ \tilde{R}_{nr}'^T \\ 0_{nr+v+1} \\ \cdots \\ 0_{nr+ns} \end{Bmatrix} \quad S_v^T = \begin{Bmatrix} 0_1 \\ \cdots \\ 0_v \\ \tilde{S}_0^T \\ \tilde{S}_1^T \\ \cdots \\ \tilde{S}_{ns}^T \\ 0_{ns+v+1} \\ \cdots \\ 0_{nr+ns} \end{Bmatrix} \tag{27}$$

with each 0_i being a pxp null matrix. Using the above relation (26) can be represented in a Toeplitz form as

$$[\, R_0^T \ldots R_{ns}^T \; -S_1^T \ldots -S_{nr}^T \,] \begin{pmatrix} S_0^T \\ S_1^T \\ \cdots \\ S_{ns}^T \\ R_1^T \\ \cdots \\ R_{nr}^T \end{pmatrix} = [\, S_1^T \,] \tag{28}$$

By solving this equation, we obtain the control law polynomials R and S.

Self Tuning Regulator

The off-line version described in the previous section assumed the knowledge of A, B, C polynomials. These are not known off hand but can be estimated. There are many algorithms available to estimate such systems depending on the type of the C polynomial. In our application, i.e. identification of dynamics in the furnace, it is

assumed that C=I and hence recursive least squares algorithm is used to identify the system parameters.

Recursive Least Squares Algorithm

The system is assumed to have a model structure as in equation (1)

$$A(z^{-1})\, y(t) = B(z^{-1})u(t) + C(z^{-1})n(t) \tag{29}$$

with all the symbols same as before. Converting (29) into the vector difference equation notation as

$$y(t) = -A_1 y(t-1) - \ldots - A_{na} y(t-na) + B_1 u(t-1) + \ldots + B_{nb} u(t-nb) + n(t) \tag{30}$$

Defining the following matrices

$$Y_v = \begin{bmatrix} y^T(-v) \\ y^T(1-v) \\ \cdots \\ y^T(N-v) \end{bmatrix} \quad U_v = \begin{bmatrix} u^T(-v-k) \\ y^T(1-v-k) \\ \cdots \\ y^T(N-v-k) \end{bmatrix} \quad V = \begin{bmatrix} n^T(1) \\ n^T(2) \\ \cdots \\ n^T(N) \end{bmatrix} \tag{31}$$

Where N is the total number of observations. Using notations in (31), y(t) for N observation is given as

$$Y_0 = [-Y_1 - Y_2 \ldots - Y_{na}\, U_0\, U_1 \ldots U_{nb}] \begin{bmatrix} A_1^T \\ A_2^T \\ \cdots \\ A_{na}^T \\ B_0^T \\ B_1^T \\ \cdots \\ B_{nb}^T \end{bmatrix} + V \tag{32}$$

Defining

$$f = [-Y_1 - Y_2 \ldots - Y_{na}\, U_0\, U_1 \ldots U_{nb}]$$

$$q = \begin{bmatrix} A_1^T \\ A_2^T \\ \cdots \\ A_{na}^T \\ B_0^T \\ B_1^T \\ \cdots \\ B_{nb}^T \end{bmatrix} \tag{33}$$

Equation (31) after taking advantage of the notations in (33) become

$$Y_0 = fq + V \tag{34}$$

The off-line least square estimate is given by

$$\hat{q} = (f^T f)^{-1} f^T Y_0 \tag{35}$$

Note that the estimate is a matrix. It takes too much time to compute this quantity every time. Hence a recursive version is developed and could be seen in [Goodwin and Sin 1984].

Defining an additional quantity

$$j_n = [-y_n^T - y_{n-1}^T \cdots - y_{n-na}^T u_{n-k}^T u_{n-k-1}^T \cdots u_{n-nb}^T] \tag{36}$$

The least square estimates are given by

$$P_{n+1} = \frac{1}{l}\left(P_n - \frac{P_n f_n f_n^T P_n}{l + f_n^T P_n f_n}\right) \tag{37}$$

$$\hat{q}_{n+1} = \hat{q}_n + \frac{P_n f_n}{l + f_n^T P_n f_n}(Y_{n+1} - f_{n+1}^T \hat{q}_n) \tag{38}$$

Complete Self-tuning Algorithm

1. Assume initial $\hat{q}_0$, $P_n = aI$, where a is a large number. We are not sure about the initial value of $\hat{q}$ and so by keeping P large, we have a high initial gain in the updation equation which result in the estimated parameters having a very fast initial convergence rate. Actually large a implies very little confidence on the initial guess of $\hat{q}_0$.
2. Past value of y and u are used to update $\hat{q}$ and P using equations (38) and (37).
3. Using $\hat{q}$, we find $\hat{A}(z^{-1})$ and $\hat{B}(z^{-1})$ from (33).
4. With this $\hat{A}(z^{-1})$ and $\hat{B}(z^{-1})$, $\tilde{R}'$ and $\tilde{S}$ are found with the help of (28).
5. Now R' and S are found using (28).

6. R' and S are the necessary matrices needed to determine the control input u(t) using (2). This input is applied to the system.
7. Repeat from step 2.

The self-tuning property of this algorithm has been proved by [Prager and Wellstead 1980]. They assumed the convergence of the system parameters to show this feature of the algorithm. The overall convergence itself is yet a subject of research even in SISO models. But many authors have shown this algorithm working on simulation and there are few practical application which have made use of this algorithm.

Stability of overall closed loop system

In the pole placement problem formulation, we have stated that the designed controller must generate a control input u(t) and the tracking error e(t) as stable sequences. In the previous section, we derived a self tuning controller based on the pole placement design. In this section, we will show that u(t) and e(t) are stable sequences.

The system , controller, transformations and pole placement design equation are given below for convenience with all the notations same as before.

System	$Ay = Bu + Cn$	(39)
Controller	$Ru = Tr - Sy$	(40)
Transformation	$R^{-1}S = \tilde{S}\tilde{R}^{-1}$	(41)
Design Equation	$A\tilde{R} + B\tilde{S} = P$	(42)

Introducing additional transformation equations

$$A^{-1}B = \tilde{B}\tilde{A}^{-1} \tag{43}$$

$$R\tilde{A} + S\tilde{B} = \tilde{P} \tag{44}$$

$\tilde{A}$ has similar structure as $\tilde{R}$ with the first term being the identity matrix and has an order n_a. Hence, in a similar fashion as in (5) and (6), the following relations can be derived.

$$\det(A) = \det(\tilde{A}) \tag{45}$$

$$\det(B) = \det(\tilde{B}) \tag{46}$$

Now equation (42) can be written as

$$P = A\tilde{R} + B\tilde{S}$$
$$= B(B^{-1}A\tilde{R} + \tilde{S}) \quad (47)$$

Using the fact in (43), (47) can be rewritten as

$$P = B(\tilde{A}\tilde{B}^{-1}\tilde{R} + \tilde{S})$$
$$= B(\tilde{A}\tilde{B}^{-1} + \tilde{S}\tilde{R}^{-1})\tilde{R} \quad (48)$$

Again using the transformation in (41), we get

$$P = B(\tilde{A}\tilde{B}^{-1} + R^{-1}S)\tilde{R}$$
$$= BR^{-1}(R\tilde{A} + S\tilde{B})\tilde{B}^{-1}\tilde{R}$$

From (44), we get

$$P = BR^{-1}\tilde{P}\tilde{B}^{-1}\tilde{R} \quad (49)$$

Hence

$$\det(P) = \det(B)\det(R^{-1})\det(\tilde{P})\det(\tilde{B}^{-1})\det(\tilde{R}) \quad (50)$$

From relations in (5), (6), (45),(46) and using the fact $\det(R^{-1}) = \frac{1}{\det(R)}$,

$$\det(P) = \det(\tilde{P}) \quad (51)$$

Equation (39) can be written as

$$y = A^{-1}Bu + A^{-1}Cn \quad (52)$$

Substituting (52) in (40) and multiplying the resulting expression by R^{-1}, we get

$$u = -R^{-1}SA^{-1}Bu + R^{-1}Tr - R^{-1}SA^{-1}Cn \quad (53)$$

Further Simplifying (53), we get

$$u = (I_m+R^{-1}SA^{-1}B)^{-1}R^{-1}Tr - (I_m+R^{-1}SA^{-1}B)^{-1}R^{-1}SA^{-1}Cn \quad (54)$$

Now $(I_m + R^{-1}SA^{-1}B)^{-1}R^{-1}$ can be simplified as

$$(I_m + R^{-1}SA^{-1}B)^{-1}R^{-1} = [R + SA^{-1}B]^{-1} \quad (55)$$

Taking advantage of transformation defined in (43), we get

$$(I_m + R^{-1}SA^{-1}B)^{-1}R^{-1} = [R + S\tilde{B}\tilde{A}^{-1}]^{-1}$$
$$= ([R\tilde{A} + S\tilde{B}]\tilde{A}^{-1})^{-1}$$
$$= \tilde{A}(R\tilde{A} + S\tilde{B})^{-1} \quad (56)$$

In a similar fashion $(I_m + R^{-1}SA^{-1}B)^{-1}R^{-1}SA^{-1}$ can be written as

$$(I_m + R^{-1}SA^{-1}B)^{-1}R^{-1}SA^{-1} = [AS^{-1}R + B]^{-1}$$
$$= [A\tilde{R}\tilde{S}^{-1} + B]^{-1}$$
$$= ([A\tilde{R} + B\tilde{S}]\tilde{S}^{-1})^{-1}$$
$$= \tilde{S}(A\tilde{R} + B\tilde{S})^{-1} \quad (57)$$

Substituting (56) and (57) in (54), u becomes

$$u = \tilde{A}\,(R\tilde{A} + S\tilde{B})^{-1}Tr - \tilde{S}\,(A\tilde{R} + B\tilde{S})^{-1}Cn \tag{58}$$

From the relation in (42) and (52), u can be written as

$$u = \tilde{A}\tilde{P}^{-1}Tr - \tilde{S}P^{-1}Cn \tag{59}$$

Since P and $\tilde{P}$ are designed and are selected as stable matrices; the resulting input sequence is stable.

Now the tracking error e is given by

$$e = r - y$$

Using the relation in (44), we get

$$e = r - A^{-1}Bu - A^{-1}Cn \tag{60}$$

Substituting the expression (58) for u in the above relation, we get

$$\begin{aligned} e &= r - A^{-1}B(\tilde{A}\,(R\tilde{A} + S\tilde{B})^{-1}Tr - \tilde{S}\,(A\tilde{R} + B\tilde{S})^{-1}Cn) - A^{-1}Cn \\ &= (I_r - A^{-1}B\tilde{A}\,(R\tilde{A} + S\tilde{B})^{-1}T)r \\ &\qquad + (A^{-1}B\,\tilde{S}\,(A\tilde{R} + B\tilde{S})^{-1} - A^{-1})\,Cn \end{aligned} \tag{61}$$

The first term can further be simplified as follows

$$\begin{aligned} &(I_r - A^{-1}B\tilde{A}\,(R\tilde{A}+S\tilde{B})^{-1}T) \\ &\qquad = (I_r - \tilde{B}\tilde{A}^{-1}\tilde{A}\,(R\tilde{A}+S\tilde{B})^{-1}T) \\ &\qquad = I_r - \tilde{B}\tilde{P}^{-1}T \end{aligned} \tag{62}$$

Similarly, the second term in equation (61) is simplified as

$$\begin{aligned} &(A^{-1}B\,\tilde{S}\,(A\tilde{R} + B\tilde{S})^{-1} - A^{-1}) \\ &\qquad = (A^{-1}B\,\tilde{S} - A^{-1}(A\tilde{R} + B\tilde{S}))\,(A\tilde{R} + B\tilde{S})^{-1} \\ &\qquad = -\tilde{R}(A\tilde{R} + B\tilde{S})^{-1} \\ &\qquad = -\tilde{R}P^{-1} \end{aligned} \tag{63}$$

Hence the tracking error e is given by

$$= (I_r - \tilde{B}\tilde{P}^{-1}T)r - \tilde{R}P^{-1}Cn \tag{64}$$

Again since P and $\tilde{P}$ are designed as stable matrices, the resulting tracking error sequence is stable. Hence, under closed loop, both the input and the error sequences are stable.

Stability of Controller

In the previous section, we proved that the overall closed loop system is stable. There are some concerns about the controller itself becoming unstable. The input is given by

$$u = R^{-1}Tr - R^{-1}Sy \tag{65}$$

R already has an integrator which corresponds to a pole at $|z| = 1$. The other poles of R may become unstable i.e. $|z| > 1$. In other words, the poles of R can be anything as there is no provision in the design that makes R necessarily stable. This is of big concern in spite of the proof on u being stable sequence irrespective of what R is. The proof assumed zero modelling errors, unlimited inputs. In practice, we always have limited inputs and especially during self tuning mode, we have modelling errors.

When saturation of the input occurs, the system is essentially operating under open loop and the resulting system may operate in an undesired manner. Even when all the poles of R are stable, the pole at $z = 1$ can cause high frequency oscillations due to a phenomenon known as integration windup. Although many practical solutions for windup are known, the presence of unstable poles in R can render these solutions ineffective. Some of the techniques to overcome windup are given in the next section. When the controller input gets saturated, the actual input applied to the system does not belong to the controller. If after sometime, the input do return to the unsaturated region, the past inputs and outputs in equation (40) do not belong to the controller itself as a result of which the output of the system can take undesirable tours.

At this point, we conclude that if all the poles of R are at least marginally stable, then we can take care of limited inputs as given in the next section.

Some Practical Solutions to Integration Windup

Integration windup occurs, when the control input demanded by the controller saturates the actuator. The easiest solution is to remove the integrator from the control loop whenever saturation in the actuator occurs. This can be done by directly solving (19) without additional constraints given in equation (10). In this situation, we have two controllers with only one controller operating at any instance.

Another scheme which is more attractive is to include another loop in the control system as given in Figure 2. This loop gets activated only when the input demanded by controller u_a. The individual loop itself can be seen in Figure 3. The transfer function between u_c and u_a is given from Figure 3.

$$u_s = u_a - u_a \tag{66}$$

and $$u_c = R^{-1}(F(u_a - u_c) + z) \tag{67}$$

Hence, the transfer function between u_a and u_c is given by

$$u_c = (R + F)^{-1}Fu_a \tag{68}$$

The main aim of this loop is to make $u_c \rightarrow u_a$ and this is done by suitably designing F so as to make (R + F) asymptotically stable. This section gives us some techniques to overcome integration windup. The effect of the new loop on the overall

stability of the closed loop system is not shown here as the purpose of this section is to list certain techniques to get around integration windup. Again, if R has unstable poles, it is quite possible that these techniques may prove ineffective.

Example

In this section, examples are given to illustrate the pole placement design procedure in diagonal and non-diagonal systems.

(a) Diagonal Case

The diagonal system is given below

$$\begin{bmatrix} 1-1.5z^{-1}+0.7z^{-2} & 0 \\ 0 & 1-1.5z^{-1}+0.7z^{-2} \end{bmatrix} y(t) = \begin{bmatrix} z^{-1}+z^{-2} & 0 \\ 0 & z^{-1}+z^{-2} \end{bmatrix} u(t) \tag{69}$$

We want to place all the poles of the system at $z=+0.5$. In order to achieve this, we have to find $\tilde{R}'$ and $\tilde{S}$ satisfying the design equation given in (21). $\tilde{R}'$. and $\tilde{S}$ are assumed to be second order polynomials. Hence P, the desired polynomial must be of 5th order as given below

$$P = \begin{bmatrix} (1-0.5z^{-1})^5 & 0 \\ 0 & (1-0.5z^{-1})5 \end{bmatrix} \tag{70}$$

Using the procedure described in the earlier section, $\tilde{R}'$ and $\tilde{S}$ are given as

$$\tilde{R}' = \begin{bmatrix} 1-0.1419z^{-1}+0.04464z^{-2} & 0 \\ 0 & 1-0.1419z^{-1}+0.04464z^{-2} \end{bmatrix}$$

and $$\tilde{S} = \begin{bmatrix} 0.142-0.241z^{-1}+0.115z^{-2} & 0 \\ 0 & 0.142-0.241z^{-1}+0.115z^{-2} \end{bmatrix}$$

(71)

(b) Non-diagonal Case

The system is given by

$$\begin{bmatrix} 1-0.5z^{-1} & 1+0.5z^{-1} \\ 1-0.5z^{-1} & 1-0.5z^{-1} \end{bmatrix} y(t) = \begin{bmatrix} z^{-1} & 0.2z^{-1} \\ 0.3z^{-1} & z^{-1} \end{bmatrix} u(t) \tag{72}$$

Again, we want to place all the poles of the system at $z=+0.5$. $\tilde{R}'$ and $\tilde{S}$ are assumed to be first order polynomials. Hence P, the desired polynomial must be of 3rd order as given below

$$P = \begin{bmatrix} (1-0.5z^{-1})^3 & 0 \\ 0 & (1-0.5z^{-1})^3 \end{bmatrix} \tag{73}$$

$\tilde{R}'$ and $\tilde{S}$ are found using equation (21) and

$$\tilde{R}' = \begin{bmatrix} 1-0.729z^{-1} & 1+0.729z^{-1} \\ 1-0.729z^{-1} & 1-0.729z^{-1} \end{bmatrix}$$

$$\text{and} \quad \tilde{S} = \begin{bmatrix} -0.574+0.575z^{-1} & -0.093+0.093z^{-1} \\ 0.344-0.344z^{-1} & -0.452+0.453z^{-1} \end{bmatrix} \tag{74}$$

Simulation of this non-diagonal system for tracking references for two different pole location 0.5 and 0.95 are given in Figures 4 and 5. While placing poles at 0.5, the resulting controller is stable and with 0.95, the controller is unstable. This controllers are made to track references, some of which cannot be achieved with the limited inputs. It can be seen from the figures that the stable controller has much more desirable characteristic than the unstable controller. There are lot of oscillations when saturation in the actuators occurs in the case of unstable controller. For this reason stable controllers are preferred.

In our application domain, there are 8 inputs and 8 outputs. It is also observed that each term is at most a 2nd order polynomial. Hence, the furnace is modelled as a 8x8 MIMO model as given below

$$y(t) = -A_1y(t-1)-A_2y(t-2)+B_1u(t-1)+B_2u(t-2)+n(t) \tag{75}$$

where y(t) and u(t) e $\mathbf{R}^{8x1}$ and A_1, A_2, B_1, B_2 e $\mathbf{R}^{8x8}$. Here the elements of matrix $\tilde{R}'$ and $\tilde{S}$ are assumed to be at most 2nd order polynomials, ie

$$\tilde{R}' = I + \tilde{R}'_1z^{-1} + \tilde{R}'_2z^{-2}$$

$$\text{and} \quad \tilde{S}' = \tilde{S}_0 + \tilde{S}_1z^{-1} + \tilde{S}_2z^{-2} \tag{76}$$

The desired polynomial matrix P is a diagonal matrix with all diagonal terms being 5th order polynomials. This is used to control a simulated furnace. Preliminary actual input-output data of the furnace under self tuning pole placement control is given in Figures 6 and 7. It can be observed that initially there is lot of fluctuation in the input and the input hitting the limits. But after some time when the estimated parameters converge the oscillations are reduced and the desired temperature level is achieved. It is also observed that there are some oscillations about the reference temperature. It is believed that these are caused due to poor estimates resulting from the poor initial guess on the system parameter.

6. APPLICATION TO CRYSTAL GROWTH FURNACE

Application of the control technique developed in this research is presented in Appendix 1.

7. CONCLUSION

In this reserach, a self-tuning pole placement control algorithm is developed for the temperature control problem in crystal growth furnaces. The algorithm is applied

successfully to control the axial temperature around the ampoule. Its suitability in controlling the temperature of a 8-zone crystal growth furnace is discussed. The stability of the overall control system is derived. Some of the robustness issues concerned with this algorithm are analyzed.

8. REFERENCES

Astrom, K. J., and Wittenmark, B., "Computer controlled systems", Prentice Hall, Englewood Cliffs, 1984.

Batur, C., Sharpless, R. B., Duval, W.M.B , Rosenthal, B.N., "Self-tuning multivariable Pole Placement Control of Multizone Crystal Growth Furnace", Journal of Adaptive Control and Signal Processing, Vol. 6, pp. 111-123, 1992.

Batur, C., Sharpless, R B, Duval, W.M.B, Rosenthal, B.N., Singh, N B, "Identification and Control of a Multizone Crystal Growth Furnace", Journal of Crystal Growth, 119, pp. 371-380, 1992.

Bourret,E.D.,Guitron J.B,Haller E.E "Evaluation of the Mellen EDG furnace for growth of large diameter GaAs single crystals in a horizontal configuration" J. of Crystal Growth 1985 (1987) pp 124-129

Chang E.C.,Wilcox R.W." Control of interface in the vertical Bridgman-Stockbarger Technique" J. of Crystal Growth Vol 21, pp135-140 ,1974

Goodwin, G. C., and Sin, K. S., "Adaptive filtering prediction and control", Prentice Hall, Englewood Cliffs, 1984.

Goodwin G.C,Sin K.S"Adaptive filtering prediction and control" John Wiley 1984.
Ljung, L., "System Identification: Theory for the user", Prentice Hall, Englewood Cliffs, 1987.

Ljung L.,Soderstrom T."Theory and practice of recursive identification" 1983 Cambridge Mass: MIT Press.

Mansour, N. E., and Linkens, D. A., "Self-tuning pole-placement multivariable control of blood pressure for post-operative patients: a model-based study", IEE proceedings, Vol. 137, No. 1, 1990.

Mikles, J., "A multi-variable self tuning controller based on pole placement design", Automatica, vol. 26, No.2, pp 293-302, 1990.

Parsey,J.M.,Thiel,F.A "A new apparatus for the controlled growth of single crystals by horizontal Bridgman techniques" J. of Crystal Growth 73. pp. 211-220 1985.

Sebek, M., and Kucera, V., " Polynomial approach to quadratic tracking in discrete linear systems", IEEE transactions on Automatic Control, Vol. 27, No. 6, 1982.

Sharpless R.B., Batur C., Duval, W.M.B., Singh, N.B. " Computer imaging based detection and quantification of solid-liquid interface during crystal growth" Proceedings of the ASME, 1990.

Taghavi K, Duval W.M.B "Inverse heat transfer analysis of Bridgman Crystal Growth" International Journal of Heat and Mass Transfer. Vol. 32 No.9 pp. 1741-1750

Wang,C.A.,Witt,A.F.,Carruthers,J.R "Analysis of crystal growth characteristics in a conventional vertical Bridgman configuration" J. of Crystal Growth 66 1984 299-308

Wellstead, P. E., Prager, D., and Zanker, P., "Pole assignment self tuning regulator", Proceeding of the IEE, Vol. 126, No. 8, pp 781-797, 1979.

Wolovich, W. A., "Linear Multivariable Systems". Springer Verlag, New York, 1974.

Journal of Crystal Growth 119 (1992) 371–380
North-Holland

JOURNAL OF CRYSTAL GROWTH

Identification and control of a multizone crystal growth furnace

C. Batur, R.B. Sharpless

Department of Mechanical Engineering, The University of Akron, Akron, Ohio 44325-3903, USA

W.M.B. Duval, B.N. Rosenthal

NASA Lewis Research Center, Cleveland, Ohio 44135, USA

and

N.B. Singh

Westinghouse Science and Technology Center, Pittsburgh, Pennsylvania 15235, USA

Received 15 October 1991; manuscript received in final form 28 January 1992

This paper presents an intelligent adaptive control system for the control of a solid–liquid interface of a crystal while it is growing via directional solidification inside a multizone transparent furnace. The task of the process controller is to establish a user-specified axial temperature profile and to maintain a desirable interface shape. Both single-input–single-output and multi-input–multi-output adaptive pole placement algorithms have been used to control the temperature. We also describe an intelligent measurement system to assess the shape of the crystal while it is growing inside a multizone transparent furnace. A color video imaging system observes the crystal in real time, and determines the position and the shape of the interface. This information is used to evaluate the crystal growth rate, and to analyze the effects of translational velocity and temperature profiles on the shape of the interface. Creation of this knowledge base is the first step to incorporate image processing into furnace control.

1. Introduction

One way to produce a crystal is to subject the pure molten compound, encapsulated inside an ampoule, to a temperature profile which includes its solidification temperature. This requires maintaining a predetermined axial and radial temperature profile around the material, despite the effects of unknown process disturbances. To maintain continuous solidification, either the ampoule or the temperature gradient is moved along the longitudinal axis of the furnace.

Singh et al. [1] have shown that the shape of the solid–liquid interface is determined by the magnitude of the imposed temperature gradient and the translational velocity of the ampoule. Minimization of thermal stresses can be achieved by maintaining a planar interface between the solid and liquid phases of the material (Chang and Wilcox [2]). Also, a planar interface can be desirable because of minimized crystalline imperfections. Recently, Taghavi and Duval [3] have studied the effects of furnace temperature profile and translational velocity on the interface shape. They also considered the inverse problem of the desired temperature profile that would result in a planar interface.

Wang et al. [4] experimented with a vertical Bridgman-type furnace where they studied the growth of gallium-doped germanium. They verified that the macroscopic growth rate was always transient and the interface remained concave with respect to solid at the translational speed of 4 mm/s.

0022-0248/92/$05.00 © 1992 – Elsevier Science Publishers B.V. All rights reserved

PRECEDING PAGE BLANK NOT FILMED

The Mellen EDG furnace (Parsey and Thiel [4]) can emulate the heat flow characteristics of the horizontal Bridgman–Stockbarger furnace without requiring the motion of the ampoule. The use of the Mellen furnace in horizontal configuration for gallium arsenide crystal has been investigated by Bourret et al. [6]. They have found that the crystalline perfection is improved by increasing the axial temperature gradient over the solid and decreasing the radial temperature gradient over the melt.

Since the shape of the interface is a significant characteristic of this process, automatic detection and quantification of this variable can play an important role in the crystal growth control. Some of the advantages include:

(1) The quantification process provides on-line information about the position and the shape of the interface. Therefore, the effects of different temperature profiles and translational speeds on the interface shape can be determined in real time.

(2) The crystal growth rate can be calculated by detecting the position of the interface.

(3) Most importantly, the interface shape information may be used as a feedback signal in the interface controller.

In summary, material structural properties are complex, time dependent phenomena of the temperature profiles and the ampoule's translational velocity. The purpose of this study is to find a real time model of the furnace and based on this model, to implement adaptive control algorithms for the interface control.

2. Identification of furnace dynamics

2.1. *Identification of single-input–single-output (SISO) models*

The following time invariant, thermal model is assumed:

$$A_i(z^{-1})\ y_i(t) = B_i(z^{-1})\ u_i(t-1) + n_i(t), \quad (1)$$

where u, y, and n are the energy inputs, temperature, and disturbance terms respectively. $A_i(z^{-1})$ and $B_i(z^{-1})$ are the polynomials of (z^{-1}) with coefficients $[a_1\ a_2\ \cdots\ a_{na}]$ and $[b_0\ b_1\ \cdots\ b_{nb}]$. They define the dynamics of each zone. The subscript i refers to a particular heating zone. The z^{-1} is the delay operator. The disturbance $n_i(t)$ is assumed to be a zero mean stationary stochastic process.

In the furnace studied, motion of the ampoule with respect to furnace changes the dynamics of each zone. This is due to the changes in the thermal capacitance in each zone. Because the ampoule's motion is slow, 2–50 cm/day, a self-tuning temperature control algorithm is employed. As shown below, the process parameters for each zone are estimated by an on-line sequential least squares algorithm (Goodwin [7]):

$$\hat{\theta}_i(t) = \hat{\theta}_i(t-1) + \frac{P_i(t-1)\ \phi_i(t-1)}{1+\phi_i^{\mathrm{T}}(t-1)\ P_i(t-1)\ \phi_i(t-1)} \times \left[y_i(t) - \hat{\theta}_i^{\mathrm{T}}(t-1)\ \phi_i(t-1)\right], \quad (2)$$

$$P_i(t) = P_i(t-1) - \frac{P_i(t-1)\ \phi_i(t-1)\ \phi_i^{\mathrm{T}}(t-1)\ P_i(t-1)}{1+\phi_i^{\mathrm{T}}(t-1)\ P_i(t-1)\ \phi_i(t-1)}, \quad (3)$$

$$\hat{\theta}_i = [a_1\ a_2\ \cdots\ a_{na}\ b_0\ b_1\ \cdots\ b_{nb}]_i^{\mathrm{T}}, \quad (4)$$

$$\phi_i(t-1) = [-y(t-1)\ -y(t-2)\ \cdots\ -y(t-na)\ u(t-1)\ u(t-2) \times \cdots\ u(t-nb)]_i^{\mathrm{T}}, \quad (5)$$

where $\hat{\theta}_i$ is the process parameter estimates and $\phi_i(t-1)$ is the data vector for zone i. The initial choices for the algorithm are $\hat{\theta}(0) = 0$ and $P(0) = \alpha I$, where α is a large number indicating little confidence on the initial estimates.

2.2. *Identification of multi-input–multi-output (MIMO) models*

The single-input–single-output (SISO) models do not explicitly account for the temperatures and input powers of the neighboring heating

zones. Changes in power and temperature of adjacent zones act as inputs to the controlled zone. Any one zone may be affected by the power and temperature of other zones, which may act as a disturbance. This phenomenon is observed through a non-proportional power distribution along the controlled furnace. The power distribution affects the amount of radiant energy transmitted into the crystal from a particular zone. For these reasons, a multivariable model has also been determined for the system.

A multivariable model takes into account the interaction between the zones. By knowing the interactions, the controller can be designed to further minimize the temperature fluctuations within the furnace. The input and output dynamics of the system are represented by the following multivariable model:

$$A(z^{-1})\ y(t) = B(z^{-1})\ u(t-1) + n(t), \qquad (6)$$

where $A(z^{-1})$ and $B(z^{-1})$ are polynomial matrices as,

$$A(z^{-1}) = I + \sum_{i=1}^{na} A_i z^{-i}, \qquad (7)$$

$$B(z^{-1}) = \sum_{i=0}^{nb} B_i z^{-i}, \qquad (8)$$

where A_i and B_i in (7) and (8) are all 8×8 matrices. For an eight-zone furnace, input–output and noise vectors are

$$y(t) = [y_1(t)\ y_2(t)\ \cdots\ y_8(t)]^{\mathrm{T}}, \qquad (9)$$

$$u(t) = [u_1(t)\ u_2(t)\ \cdots\ u_8(t)]^{\mathrm{T}}, \qquad (10)$$

$$n(t) = [n_1(t)\ n_2(t)\ \cdots\ n_8(t)]^{\mathrm{T}}. \qquad (11)$$

Note that this multivariable model is drastically different from that of the single input single output. Zone interactions are explicitly modeled in (6) as off diagonal terms of the A_i and B_i matrices. The SISO model, on the other hand, tries to accommodate these interactions by additional noise term in the model

The multivariable model is determined by the sequential least squares algorithm. The multivariable algorithm can be obtained by replacing scalar quantities with their corresponding matrices and by following the steps outlined in (2) and (3) (Ljung [8]). In particular, the estimate and the data matrices take the following forms:

$$\hat{\theta} = [A_1\ A_2\ \cdots\ A_{na}\ B_0\ B_1\ \cdots\ B_{nb}]^{\mathrm{T}}, \qquad (12)$$

$$\phi(t-1) = [-y(t-1)\ -y(t-2)\ \cdots\ -y(t-na)\ u(t-1)\ u(t-2)\ \times\ \cdots\ u(t-nb)]^{\mathrm{T}}. \qquad (13)$$

2.3. Identification of interface shape by image processing

When the material ($PbBr_2$) solidifies, there is a distinct color change from dark red (liquid) to a light yellow (solid). The image processing methodology makes use of this information to determine the shape of the interface. For acousto-optic materials, such as lead halides, there is also an observable change in color that can be used to detect the interface.

2.3.1. Detection of interface

Hue, saturation and intensity (HSI) are the three basic components that define the color. Significant changes in any one of these components can be used to detect the edges of an object. There exist many different methodologies to accomplish this. These may include (Gonzales and Wintz [9] and Wahl [10]):

(1) histogram based segmentation;
(2) edge detection by gradient;
(3) edge models.

In this study, we investigated all three methods of edge detection. We selected the edge model based detection procedure for the interface quantification because of its robustness.

2.3.2. Heuckel edge model

Edge models are a means of fitting parameterized templates to an image. They offer an approach to position a particular optimal curve to fit a certain bounded region within an image. The method used was originally known as the Heuckel

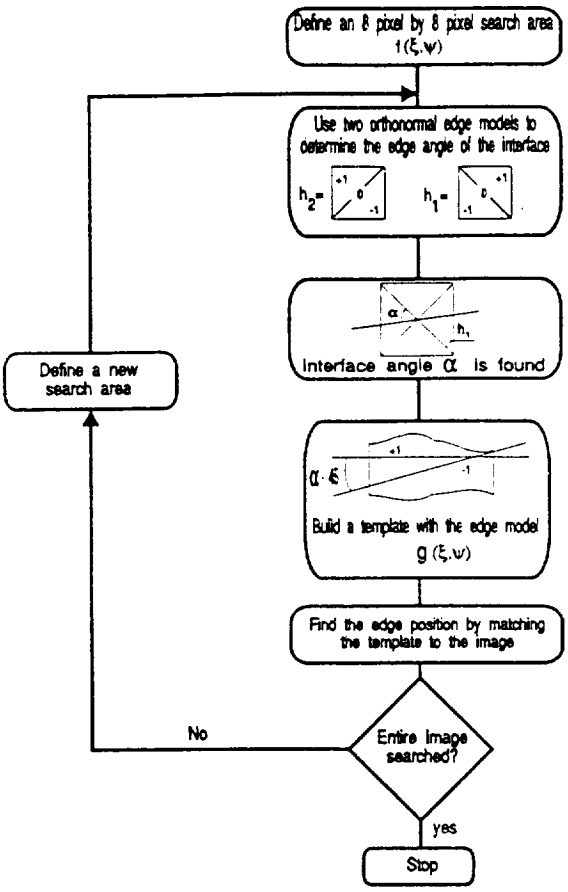

Fig. 1. Flow chart for image processing.

edge model [11]. The model is used to find an optimal line within a region and it gives an indication of the strength of the edge. The method we used is a two-step process as shown in fig. 1. The steps are described below.

Step 1: Optimum edge angle

This method was derived using Heuckel's edge model by Merro and Vassey [12]. They show that the edge angle of the best fit line (α) of an 8×8 region can be found by convolving two orthonormal bases, h_1 and h_2, as shown below:

$$\tan \alpha = \frac{\sum\sum f(\xi, \psi)\ h_2(\xi, \psi)}{\sum\sum f(\xi, \psi)\ h_1(\xi, \psi)}, \tag{14}$$

where $f(\xi, \psi)$ is the image intensity of the local coordinates within the operator's window, and α is the edge angle with respect to h_1. The orthogonal bases, h_1 and h_2, are shown in fig. 1.

Step 2: Position of the edge

Now that the optimal edge angle (α) is known, it is necessary to find the position of the edge. The angle α is used to make an edge model template $g(\xi, \psi)$. Next, the squared error between the image $f(\xi, \psi)$ and the template $g(\xi, \psi)$ is minimized by the following error measure:

$$\varepsilon = \sum\sum \left[f(\xi, \psi) - g(\xi, \psi) \right]^2, \tag{15}$$

$$\varepsilon = \sum\sum \left[f(\xi, \psi)^2 - 2 f(\xi, \psi)\ g(\xi, \psi) + g(\xi, \psi)^2 \right]. \tag{16}$$

This measure can be minimized by maximizing

$$\rho = \sum\sum f(\xi, \psi)\ g(\xi, \psi). \tag{17}$$

The point (ξ, ψ) that maximizes (17) determines the edge position. Details of the algorithm can be found in Sharpless et al. [13].

2.3.3. Determination of interface shape

Once the solid–liquid interface is found, it becomes necessary to transform the interface information into a more directly useful form. This transform should compress the data into one or more control variables which may be used to determine the quality of the crystal being produced. This shape may fall into one of the following three classes: flat, concave, or convex.

The shape can be determined by using radius of curvature at several points along the edge. The sign of the radius of curvature gives a measurement of convexity or concavity. The magnitude of the radius is a gauge of the amount of curvature.

3. Furnace control

3.1. Self-tuned pole placement temperature controller, SISO case

The control law for the process is assumed to be

$$R(z^{-1})\ u(t) = T(z^{-1})\ r(t) - S(z^{-1})\ y(t), \tag{18}$$

where $R(z^{-1})$, $T(z^{-1})$, and $S(z^{-1})$ are polynomi-

als to be determined. Substituting (18) into the process dynamics (1) and solving for $y(t)$, gives

$$y(t) = \frac{B(z^{-1})\ T(z^{-1})}{A(z^{-1})\ R(z^{-1}) + B(z^{-1})\ S(z^{-1})} r(t). \tag{19}$$

If the desired characteristic polynomial for the feedback control system is $P(z^{-1})$, it follows from (19) that

$$A(z^{-1})\ R(z^{-1}) + B(z^{-1})\ S(z^{-1}) = F(z^{-1})\ P(z^{-1}), \tag{20}$$

where $F(z^{-1})$ is an observer polynomial. To guarantee zero steady state error for step input, the controller is designed to have an integrator, i.e.,

$$R(z^{-1}) = (1 - z^{-1})\ R_f(z^{-1}). \tag{21}$$

Then, by defining proper $F(z^{-1})$ and $P(z^{-1})$, $R_f(z^{-1})$ and $S(z^{-1})$ can be solved by equating corresponding powers of z^{-1} in (20).

The reference filter $T(z^{-1})$ is solved by considering the steady state relation between $r(t)$ and $y(t)$. Since $R(1) = 0$, it follows from (19) that in the steady state:

$$\bar{y} = \frac{B(1)\ T(1)}{B(1)\ S(1)} \bar{r} = \frac{T(1)}{S(1)} \bar{r}. \tag{22}$$

If $T(1) = S(1)$, then $\bar{y} = \bar{r}$ in the steady state.

3.2. *Self-tuned pole placement temperature controller, MIMO case*

The control law used in the multivariable case has the same form as in (18). However, the scalar polynomials R, T, and S are replaced by matrix polynomials. Substituting (18) into (6), the closed loop process equation becomes

$$Ay(t) = BR^{-1}[Tr(t) - Sy(t)] + n(t). \tag{23}$$

Arranging for $y(t)$ gives

$$[A + BR^{-1}S]\ y(t) = z^{-1}\ BR^{-1}T\ r(t) + n(t), \tag{24}$$

$$R^{-1}S = \tilde{S}\tilde{R}^{-1}, \tag{25}$$

with $nr = n\tilde{r}$ and $ns = n\tilde{s}$. Then, (24) can be written as

$$\left[A\tilde{R} + B\tilde{S}\right]\tilde{R}^{-1}\ y(t) = z^{-1}\ BR^{-1}T\ r(t) + n(t). \tag{26}$$

The solution for R, S, and T follows a similar approach as in the case of SISO design, by setting

$$\left[A\tilde{R} + B\tilde{S}\right] = I + P_1 z^{-1} + P_1 z^{-1} + \cdots + P_{np} z^{-np} = P(z^{-1}), \tag{27}$$

where $P(z^{-1})$ is the designer's closed loop characteristic polynomial with each P_i as an 8×8 matrix. The order of $P(z^{-1})$ is determined by the model order and the controller order as

$$np = \max\{na + nr,\ 1 + nb + ns\}. \tag{28}$$

By imposing zero steady state error, the T polynomial can be solved similar to the SISO case. By setting

$$\tilde{R} = (I - Iz^{-1})\tilde{R}_f, \tag{29}$$

the steady state solution for (26) is

$$\left[A(1)\ \tilde{R}(1) + B(1)\ \tilde{S}(1)\right]\ \tilde{R}^{-1}(1)\ \bar{y}(t) = B(1)\ R^{-1}(1)\ T(1)\ \bar{r}(t). \tag{30}$$

Using (25) and (29), (30) becomes

$$R^{-1}(1)\ S(1)\ \bar{y} = R^{-1}(1)\ T(1)\ \bar{r}. \tag{31}$$

With the choice of $T(1) = S(1)$, eq. (31) becomes $\bar{y}(t) = \bar{r}(t)$ in the steady state.

In order to implement the control law, $\tilde{R}$ and $\tilde{S}$ must be transformed to R and S using (25), i.e.

$$S\tilde{R} = R\tilde{S}. \tag{32}$$

4. Experimental results

The major motivations behind the experimental study are:

(A) Comparison between the SISO and MIMO self tuning temperature control algorithms.

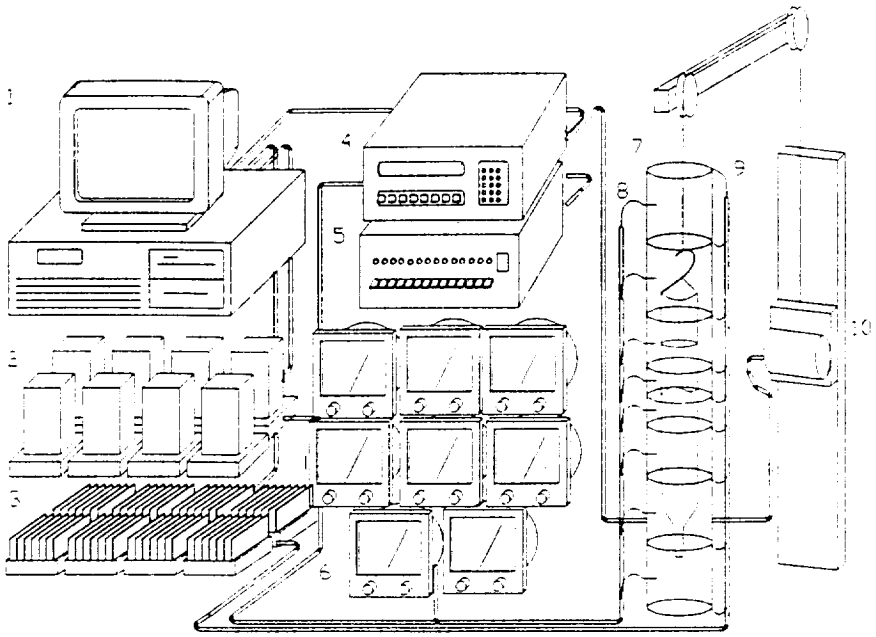

Fig. 2. Temperature control hardware: (1) computer controller with A/D and D/A boards; (2) thermocouple transducers; (3) duty cycle based heater drivers; (4) translational mechanism controller; (5) independent data acquisition system; (6) independent on–off controller for safety; (7) transparent furnace; (8) thermocouples; (9) heater connections; (10) translational mechanism.

(B) Image processing based quantification of the interface.

Fig. 2 shows the temperature control system. The furnace has eight interacting heating zones and in each zone the temperature is measured by three K type thermocouples. Based on 12 bit A/D conversion and a measurement range of 700°C, the temperature reading resolution is

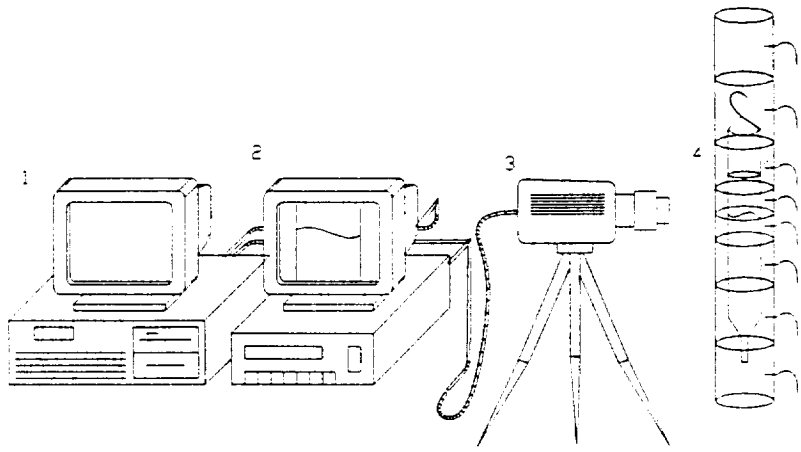

Fig. 3. Image processing hardware: (1) computer; (2) intermittent video recorder and video monitor; (3) TV camera and front-end lens system; (4) furnace.

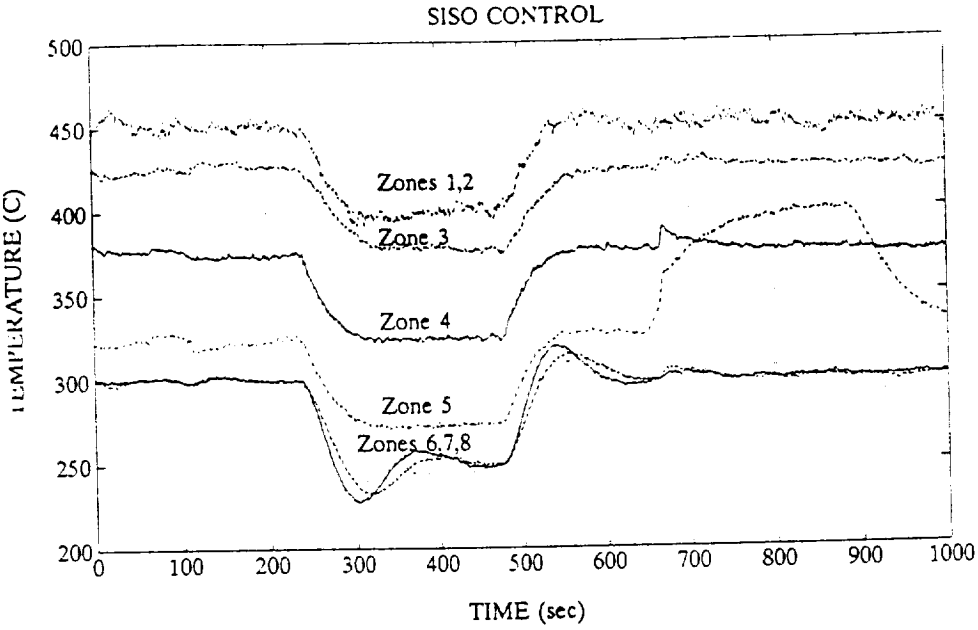

Fig. 4. Furnace operating under SISO control.

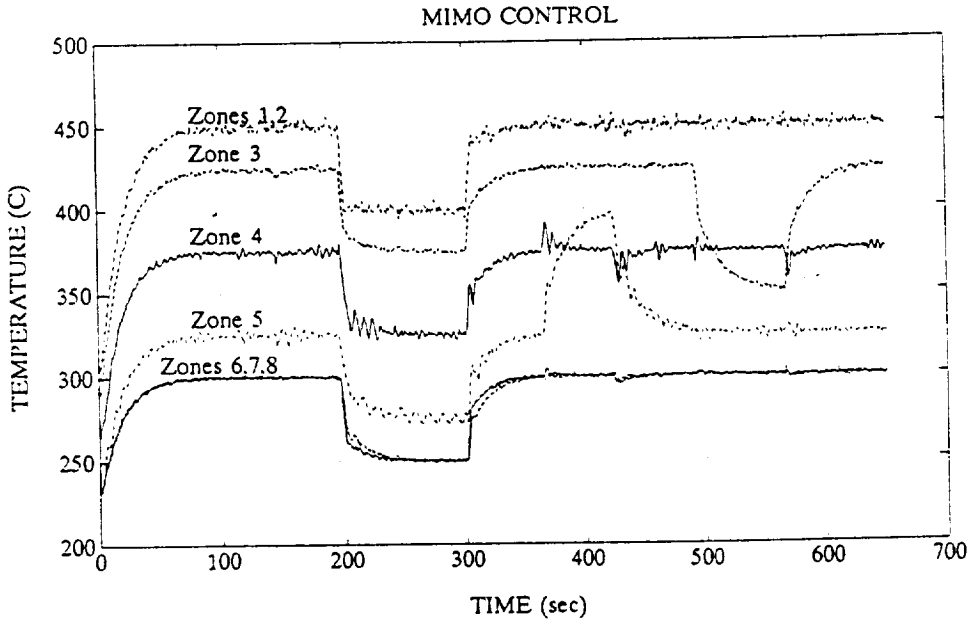

Fig. 5. Furnace operating under MIMO control.

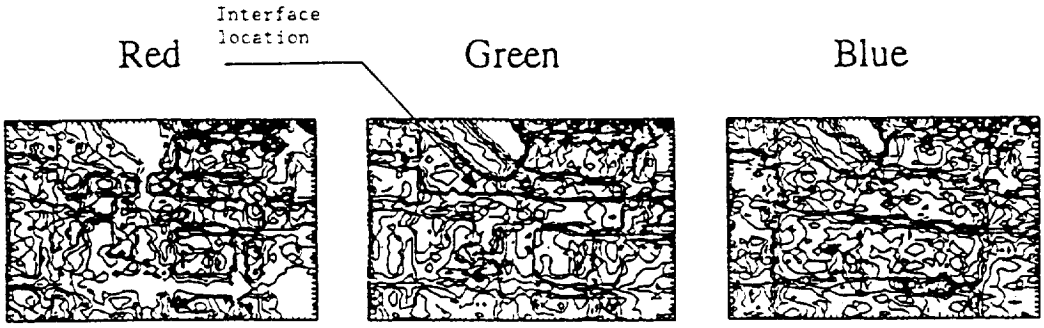

Fig. 6. Color component contour plots.

0.12°C. The heater drivers are zero crossing, duty cycle modulated solid state switches. Each can be driven from a D/A port of the computer with a 12 bit resolution. The main disturbance on the control system is the motion of the ampoule. This is provided by a computer controlled translational mechanism. The motion resolution on this system is approximately 1 μm per step.

The imaging system is shown in fig. 3. It can provide a view of the interface with an eight-bit resolution on each color. The total number of pixels representing the image is 512×480.

Figs. 4 and 5 show the performance of the control system both in SISO and in MIMO self-tuning mode. In each case, two different experiments are performed:

(1) For the first experiment, all reference temperatures are first decreased and then increased simultaneously by 50°C. The aim of this experiment is to see if the response follows the curve imposed by the desired pole locations.

(2) The second experiment is designed to see the effect of zone to zone interactions. Only one reference temperature is changed by 75°C, all

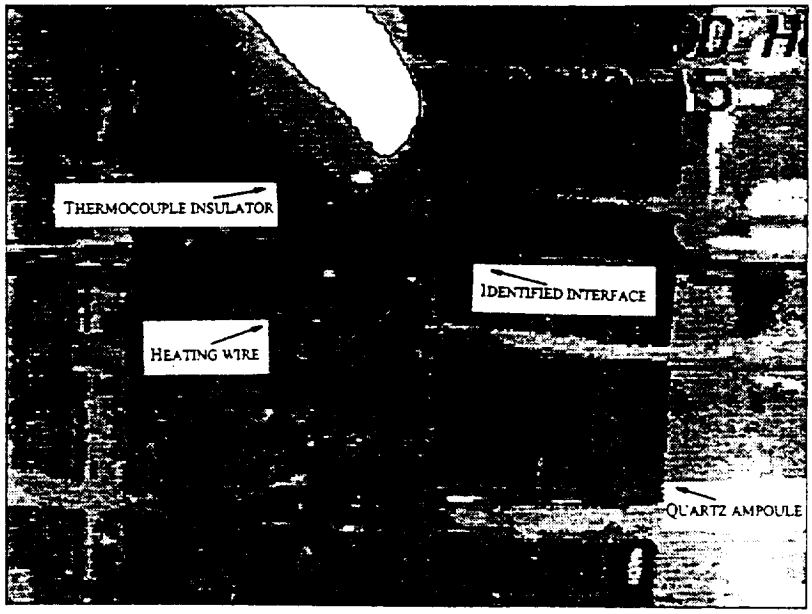

Fig. 7. End result of interface identification.

others are kept constant. For both SISO and MIMO control, the desired poles are placed at location $z = 0.9$. This choice results in an overdamped response.

The results of these experiments lead to the following conclusions:

(a) In MIMO control, all zones behave in a similar pattern. This pattern is imposed by the desired pole locations. In the case of SISO control, zones 6, 7, and 8 show underdamped responses. This illustrates that the SISO pole placement design cannot handle zone-to-zone interaction as expected.

(b) In the case of MIMO control, if one zone's reference temperature is changed, this change has an effect on the neighboring zones. However, the effect is not long lasting in comparison with the same changes introduced in the case of SISO control.

(c) There is no noticeable difference between the SISO and MIMO controllers in the steady state operation.

The image quantification starts with the red, green, and blue components of the image. Fig. 6 shows these components around the interface. As it can be observed, the green component provides the greatest contrast around the interface. This is illustrated by the close fit contour lines which show the interface better in the green than in the red and blue components. The Heuckel algorithm outlined in fig. 1 is applied to the green component of the picture. The resulting image is shown in fig. 7 where the identified interface is marked by a bold black line. The speed of the algorithm is approximately 5 s, which is properly suited to the time step within the temperature control algorithm. During this time the algorithm finds the interface within an 8×255 pixel region.

5. Conclusion

This paper presents an innovative approach, employing image processing techniques in connection with the conventional identification procedures to identify and control the dynamics of a crystal while it is growing inside a transparent furnace.

A multizone transparent crystal growth furnace is controlled by an adaptive pole placement controller. Changes in the furnace dynamics and the interaction between neighboring heating zones are estimated by an on-line least squares algorithm. The pole placement control algorithm is extensively tested on the growth of lead bromide crystals.

For an explicit model of the heat interactions between heating zones, a multi-input–multi-output (MIMO) model is determined. A self-tuning multivariable regulator is developed and applied to the furnace. Comparison between the resulting single-input–single-output (SISO) and MIMO controllers is performed. This comparison shows that the MIMO controller provides better control in eliminating zone-to-zone heat interactions. This is important because it avoids local overheating of any zone due to interaction. Thereby, a much smoother temperature profile structure can be imposed.

Several different image processing routines have been applied to find the solid–liquid interface while a crystal is growing within a transparent furnace. A technique based on the Heuckel edge model is found to be the most effective means to determine the position and shape of the interface. This shape information can be used to assess the quality of a crystal while it is growing.

Acknowledgement

This work is supported by NASA Lewis Research Center, Processing Science Technology Branch.

References

[1] N.B. Singh, W.M.B. Duval and B.N. Rosenthal, J. Crystal Growth 89 (1988) 80.
[2] C.E. Chang and W.R. Wilcox, J. Crystal Growth 21 (1974) 135.
[3] K. Taghavi and W.M.B. Duval, Intern. J. Heat Mass Transfer 32 (1989) 1741.
[4] C.A. Wang, A.F. Witt and J.R. Carruthers, J. Crystal Growth 66 (1984) 299.
[5] J.M. Parsey, Jr. and F.A. Thiel, J. Crystal Growth 73 (1985) 211.

[6] E.D. Bourret, J.B. Guitron and E.E. Haller, J. Crystal Growth 85 (1987) 124.
[7] G.C. Goodwin and K.S. Sin, Adaptive Filtering Prediction and Control (Prentice-Hall, Englewood Cliffs, NJ, 1985).
[8] L. Ljung, System Identification (Prentice-Hall, Englewood Cliffs, NJ, 1987).
[9] R.C. Gonzalez and P. Wintz, Digital Image Processing, 2nd ed. (Addison-Wesley, Reading, MA, 1987).
[10] F.M. Wahl, Digital Image Signal Processing (Atrech House, 1987).
[11] M.H. Heuckel, J. Assoc. Comput. Mach. 18 (1971) 113.
[12] L. Merro and Z. Vassay, A simplified and fast version of the Heuckel operator for finding optimal edges in pictures, in: Proc. 4th Intern. Conf. on Artificial Intelligence, 1975.
[13] R.B. Sharpless, C. Batur, W.M.B. Duval, B.N. Rosenthal and N.B. Singh, Computer based imaging detection and quantification of solid-liquid interface during crystal growth, in: Proc. ASME Winter Annual Meeting, 1990.

National Aeronautics and
Space Administration

Lewis Research Center
Cleveland, Ohio
44135

NASA

8/4/93 Send copy to P.I. and Lois Smith to follow up & file as Grant file. Cs

Reply to Attn of: 1520

July 28, 1993

RECEIVED
JUL 30 1993
RESEARCH SERVICES
THE UNIVERSITY OF AKRON

University of Akron
Office of Research Services
and Sponsored Programs
Akron, OH 44325-2102

Subject: Closeout Documents, NCC3-150, P.I., C. Batur

The period of performance under the subject cooperative agreement expired November 30, 1991.

In our letter dated, May 26, 1992, we requested certain documents in order to closeout the subject cooperative agreement and retire our file. According to our records we have not received the following materials:

1. Delivery of the Final Technical Report distributed as follows:

   a. Orginial to Grants Officer, Mail Stop 500-215.
   b. Copy to NASA Technical Officer.
   c. Copy to NASA Center for Aerospace Information, P.O. Box 8757, BWI Airport, MD 21240.

2. Submission of the final equipment inventory report, a negative report is required should no inventory exist.

If complaince has been made, please send copies to the attention of Pat Justice, Procurement Assistant, Mail Stop 500-315. Thank you for your assistance.

Saundra Gage

Saundra Gage
Grants Officer